THE JOURNAL OF BIOLOGICAL CHEMISTRY
Vol. 279, No. 29, Issue of July 16, pp. 30563–30572, 2004

Printed in U.S.A.

Atomic Resolution Structures and Solution Behavior of Enzyme-Substrate Complexes of *Enterobacter cloacae* PB2 Pentaerythritol Tetranitrate Reductase

MULTIPLE CONFORMATIONAL STATES AND IMPLICATIONS FOR THE MECHANISM OF NITROAROMATIC EXPLOSIVE DEGRADATION*

Received for publication, March 31, 2004
Published, JBC Papers in Press, May 5, 2004, DOI 10.1074/jbc.M403541200

Huma Khan‡§, Terez Barna‡§, Richard J. Harris‡, Neil C. Bruce¶, Igor Barsukov‡, Andrew W. Munro‡, Peter C. E. Moody‡, and Nigel S. Scrutton‡‖

From the ‡Department of Biochemistry, University of Leicester, University Road, Leicester LE1 7RH, United Kingdom and the ¶Centre for Novel Agricultural Products, Department of Biology, University of York, York YO10 5YW, United Kingdom

The structure of pentaerythritol tetranitrate (PETN) reductase in complex with the nitroaromatic substrate picric acid determined previously at 1.55 Å resolution indicated additional electron density between the indole ring of residue Trp-102 and the nitro group at C-6 of picrate. The data suggested the presence of an unusual bond between substrate and the tryptophan side chain. Herein, we have extended the resolution of the PETN reductase-picric acid complex to 0.9 Å. This high-resolution analysis indicates that the active site is partially occupied with picric acid and that the anomalous density seen in the original study is attributed to the population of multiple conformational states of Trp-102 and not a formal covalent bond between the indole ring of Trp-102 and picric acid. The significance of any interaction between Trp-102 and nitroaromatic substrates was probed further in solution and crystal complexes with wild-type and mutant (W102Y and W102F) enzymes. Unlike with wild-type enzyme, in the crystalline form picric acid was bound at full occupancy in the mutant enzymes, and there was no evidence for multiple conformations of active site residues. Solution studies indicate tighter binding of picric acid in the active sites of the W102Y and W102F enzymes. Mutation of Trp-102 does not impair significantly enzyme reduction by NADPH, but the kinetics of decay of the hydride-Meisenheimer complex are accelerated in the mutant enzymes. The data reveal that decay of the hydride-Meisenheimer complex is enzyme catalyzed and that the final distribution of reaction products for the mutant enzymes is substantially different from wild-type enzyme. Implications for the mechanism of high explosive degradation by PETN reductase are discussed.

Pentaerythritol tetranitrate (PETN)[1] reductase is a member of the old yellow enzyme (OYE) family of flavoproteins and was purified from a strain of *Enterobacter cloacae* (strain PB2) originally isolated on the basis of its ability to utilize nitrate ester explosives such as PETN and glycerol trinitrate (GTN) as sole nitrogen source (1). The structure of PETN reductase (2) is similar to that of OYE (3) and morphinone reductase (4), confirming the close evolutionary relationship with OYE and other FMN-dependent flavoprotein oxidoreductases inferred from sequence analysis of the genes encoding these enzymes (5, 6). Consistent with this close relationship is the ability of the OYE family of enzymes to reduce a variety of cyclic enones, including 2-cyclohexenone and steroids. Some steroids act as substrates, whereas others are potent inhibitors of these enzymes. PETN reductase, and the related orthologues from strains of *Pseudomonas* (7) and *Agrobacterium* (8), show reactivity against explosive substrates. PETN reductase degrades major classes of explosive, including nitroaromatic compounds (*e.g.* trinitrotoluene TNT) and nitrate esters (GTN and PETN) (9–11). Degradation of TNT involves reductive hydride addition to the aromatic nucleus (Fig. 1). In the case of members of the old yellow enzyme family of enzymes that are closely related to PETN reductase, the products of TNT reduction have been shown to result from both reductive hydride addition at the aromatic nucleus and also nitro group reduction in two competing pathways in the oxidative half-reaction of the enzyme (9, 12, 13). The reaction of PETN reductase comprises two half-reactions: in the reductive half-reaction, enzyme is reduced by NADPH to yield the dihydroquinone form of the enzyme-bound FMN, and in the oxidative half-reaction the flavin is oxidized by the nitro-containing explosive substrates or cyclic enone substrates. A detailed kinetic mechanism based on stopped-flow data has been proposed (14), and recently hydride transfer in the reductive half-reaction was shown to proceed by quantum mechanical tunneling (15).

The structures of PETN reductase in complex with steroid substrates and inhibitors have been determined (2), as have complexes of the enzyme with 2-cyclohexenone, the inhibitor 2,4-dinitrophenol (2,4-DNP), and the substrates TNT and picric acid (14). The 1.55 Å structure of the enzyme in complex with picric acid indicated additional electron density between the indole ring of residue Trp-102 and the nitro group at C-6 of picrate, which at this resolution suggested the presence of an

* This work was funded by grants from the UK Biotechnology and Biological Sciences Research Council, the Wellcome Trust, and the Lister Institute of Preventive Medicine. The costs of publication of this article were defrayed in part by the payment of page charges. This article must therefore be hereby marked "*advertisement*" in accordance with 18 U.S.C. Section 1734 solely to indicate this fact.

The atomic coordinates and structure factors (code 1vyr, 1vyp, and 1vys) have been deposited in the Protein Data Bank, Research Collaboratory for Structural Bioinformatics, Rutgers University, New Brunswick, NJ (http://www.rcsb.org/).

§ The first two authors contributed equally to the work.

‖ A Lister Institute Research Professor. To whom correspondence should be addressed. Tel.: 44-116-223-1337; Fax: 44-116-252-3369; E-mail: nss4@le.ac.uk.

[1] The abbreviations used are: PETN, pentaerythritol tetranitrate; TNT, trinitrotoluene; GTN, glycerol trinitrate; OYE, old yellow enzyme; 2,4-DNP, 2,4-dinitrophenol.

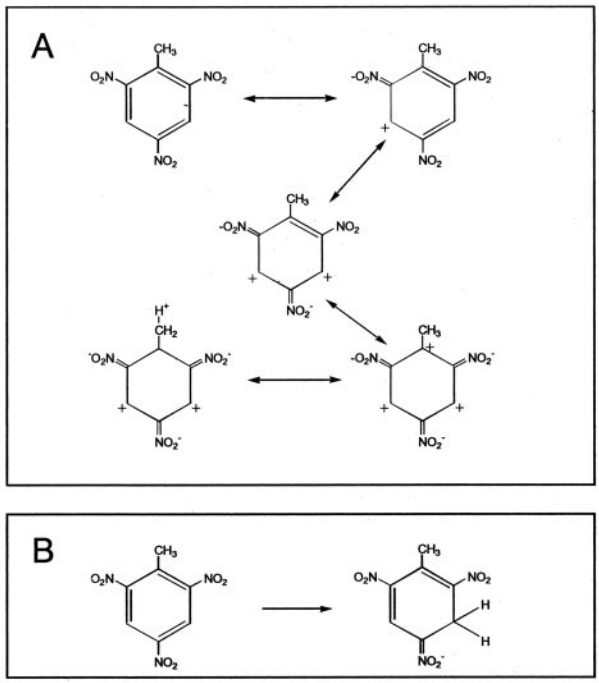

FIG. 1. **Resonance forms of TNT.** *Panel A*, structure of TNT as the resonance hybrid of several canonical forms, illustrating the enhancement in the electrophilicity of C3 and C5, the site of hydride ion addition. *Panel B*, reduction of TNT by PETN reductase to form the Meisenheimer-hydride complex.

unusual bond between substrate and the tryptophan side chain (14). The formation of such an unusual bond would clearly have profound implications for the mechanism of picric acid and TNT reduction in the enzyme. Thus, to address the origin of the additional electron density observed between residue Trp-102 and picric acid, in this paper we have extended the resolution of the wild-type enzyme in complex with picric acid to 0.9 Å. Our high resolution studies reveal that the additional density observed in the 1.55 Å structure of the wild-type-picric acid complex is attributed to the population of multiple conformational states of Trp-102 and not a formal covalent bond between the indole ring of Trp-102 and picric acid. To understand further the reaction mechanism of PETN reductase, and in particular the role of Trp-102, we have mutated this residue to phenylalanine (W102F) and tyrosine (W102Y) and we describe detailed kinetic studies of these mutant PETN reductases. Solution studies indicate that exchange of Trp-102 for tyrosine and phenylalanine favors the binding of picric acid through the removal of steric constraints, an aspect also confirmed by determination of the crystal structures of these enzymes bound to picric acid. Kinetic and NMR studies with the mutant and wild-type enzymes indicate that removal of the indole side chain also influences the distribution of the reaction products with the nitroaromatic substrate TNT. The role of Trp-102 in catalysis by PETN reductase and related enzymes, and implications for the partitioning of reaction pathways in nitroaromatic reduction, are discussed.

EXPERIMENTAL PROCEDURES

Chemicals—All chemicals were of analytical grade where possible. Complex bacteriological media were from Unipath, and all media were prepared as described in Sambrook *et al.* (16). Mimetic Orange 2 affinity chromatography resin was from Affinity Chromatography Ltd. Q-Sepharose resin was from Amersham Biosciences. NADPH, glucose 6-phosphate dehydrogenase, glucose 6-phosphate, benzyl viologen, methyl viologen, 2-hydroxy-1,4-naphthaquinone, phenazine methosulfate and 2,4-DNP were from Sigma. 2-Cyclohexenone was from Acros Organics. Dr. S. Nicklin (UK Defense and Evaluation Research Agency) supplied TNT, GTN, and picric acid. The following extinction coefficients were used to calculate the concentration of substrates and enzyme: NADPH ($\epsilon_{340} = 6.22 \times 10^3$ M^{-1} cm^{-1}); PETN reductase ($\epsilon_{464} = 11.3 \times 10^3$ M^{-1} cm^{-1}). Stock solutions of TNT (600 mM) were made up in acetone. Dilutions were then made into 50 mM potassium phosphate buffer, pH 7.0, and the acetone concentration was maintained at 1% (v/v). The presence of acetone in buffers at 1% (v/v) was shown not to affect enzyme activity.

Mutagenesis and Protein Purification—Site-directed mutagenesis of Trp-102 was achieved using the QuikChange mutagenesis method (Stratagene) and the following oligonucleotides (and their complementary sequences): 5′-CGG TTC AGC TGT TTC ACA CCG GTC G-3′ (W102F forward primer), 5′-CGA CCG GTG TGA AAC AGC TGA ACC G-3′ (W102F, reverse primer), 5′-CGG TTC AGC TGT ATC ACA CCG GTC G-3′ (W102Y, forward primer), and 5′-CGA CCG GTG TGA TAC AGC TGA ACC G-3′(W102Y, reverse primer). Plasmid pONR1 (6) was used as template for mutagenesis reactions. All mutant genes were completely sequenced to ensure that spurious changes had not arisen during the mutagenesis reaction. The expression and purification of the wild-type and mutant PETN reductase enzymes was as described previously for wild-type enzyme (6).

Redox Potentiometry Ligand Binding and Kinetic Analyses—Redox titrations and the determination of redox potential of the enzyme-bound FMN were performed as described previously for wild-type PETN reductase (14).[2] Ligand binding studies were also as performed previously with wild-type PETN reductase (14), relying on the perturbation of the flavin electronic absorption spectrum on binding ligand in the active site of PETN reductase. Data were collected in the UV-visible region (250–600 nm), and the absorption at 518 nm plotted as a function of ligand concentration. Data in the plots were analyzed by fitting to Equation 1,

$$\Delta A = \frac{\Delta A_{max}}{2E_T}[(L_T + E_T + K_d) - ((L_T + E_T + K_d)^2 - (4L_T E_T))^{0.5}] \quad \text{(Eq. 1)}$$

where ΔA_{max} is the maximum absorption change at 518 nm, L_T is the total ligand concentration and E_T the total enzyme concentration. Rapid reaction kinetic experiments using single wavelength absorption and photodiode array detection were performed using an Applied Photophysics SF.17MV stopped-flow instrument contained within an anaerobic glove box as described previously for wild-type PETN reductase (14).

Multiple Turnover Studies and NMR Analysis of Reaction Products—Multiple turnover studies were performed under anaerobic conditions and the reaction progress monitored by absorption spectroscopy. The reaction mix (total volume, 1 ml) comprised 0.2 μM PETN reductase, 30 μM NADPH, and 100 μM TNT contained in 50 mM potassium phosphate buffer, pH 7.0, and reactions were performed at 25 °C. A NADPH-generating system comprising 10 mM glucose 6-phosphate, and 1 unit of glucose-6-phosphate dehydrogenase was also included in the reaction mix. UV-visible spectra were recorded using a Jasco V530 spectrophotometer contained within a Belle Technology anaerobic glove box. Multiple turnover studies were also performed directly in the NMR instrument. Reference one- and two-dimensional COSY proton spectra were collected for the reaction components. The reaction mixture of 1 mM TNT, 0.2 μM PETN reductase, 1.5 mM NADPH, in the D_2O buffer (50 mM potassium phosphate, pH 7.0) was transferred into the NMR tube under anaerobic conditions, and a series of one-dimensional NMR spectra were collected at 5-min intervals. Upon completion of the reaction, as evidenced by the absence of changes in the NMR spectra, a two-dimensional COSY spectrum was acquired. The dead time of the reaction between the mixing of the components and the acquisition of the first one-dimensional spectrum was ~10 min. All spectra were acquired at 600 MHz on a Bruker DRX600 spectrometer at 25 °C. The spectra were processed and analyzed using XWINNMR 3.5 software (Bruker), and were referenced to the external DSS standard at 0.000 ppm.

Crystallography—Crystals of wild-type, W102F, and W102Y PETN

[2] In Ref. 14 the midpoint reduction potential for the concerted two electron reduction of wild-type PETN reductase is reported as −195 ± 5 mV. We have shown subsequently that this value is incorrect because of incorrect calibration of the electrode used in potentiometric analysis. Correct values for wild-type PETN reductase (−267 ± 5 mV) and the W102Y (−236 ± 5 mV) and W102F (−241 ± 5 mV) enzymes were determined and reported herein. The spectral changes occurring during redox titration of the wild-type enzyme were identical to those reported in Ref. 14; similar spectral changes were also observed for the W102Y and W102F enzymes.

TABLE I
Data collection and refinement statistics for PETN reductase

	Wild type	W102Y	W102F
Total observations	998,709	78,865	332,712
Unique reflections	254,704	29,340	91,259
Resolution (Å)[a]	0.90 (0.94–0.90)	1.8 (1.86–1.80)	1.27 (1.32–1.27)
Completeness (%)[a]	94.8 (65.7)	89.9 (92.7)	93.8 (90.4)
R_{merge} (%)[a]	8.7 (44.0)	5.2 (22.4)	5.5 (26.0)
$I/\text{sig}(I)$	29.7 (2.4)	10.3 (2.2)	17.1 (2.5)
R_{work}	13.2 (32.6)	14.2 (19.3)	13.3 (17.3)
R_{free}	14.3 (30.9)	19.9 (28.1)	15.3 (22.3)
Root mean square deviations from ideal			
Bond lengths (Å)	0.012	0.022	0.014
Bond angles (°)	1.62	1.87	1.48

[a] Values in parentheses for the outer bin.

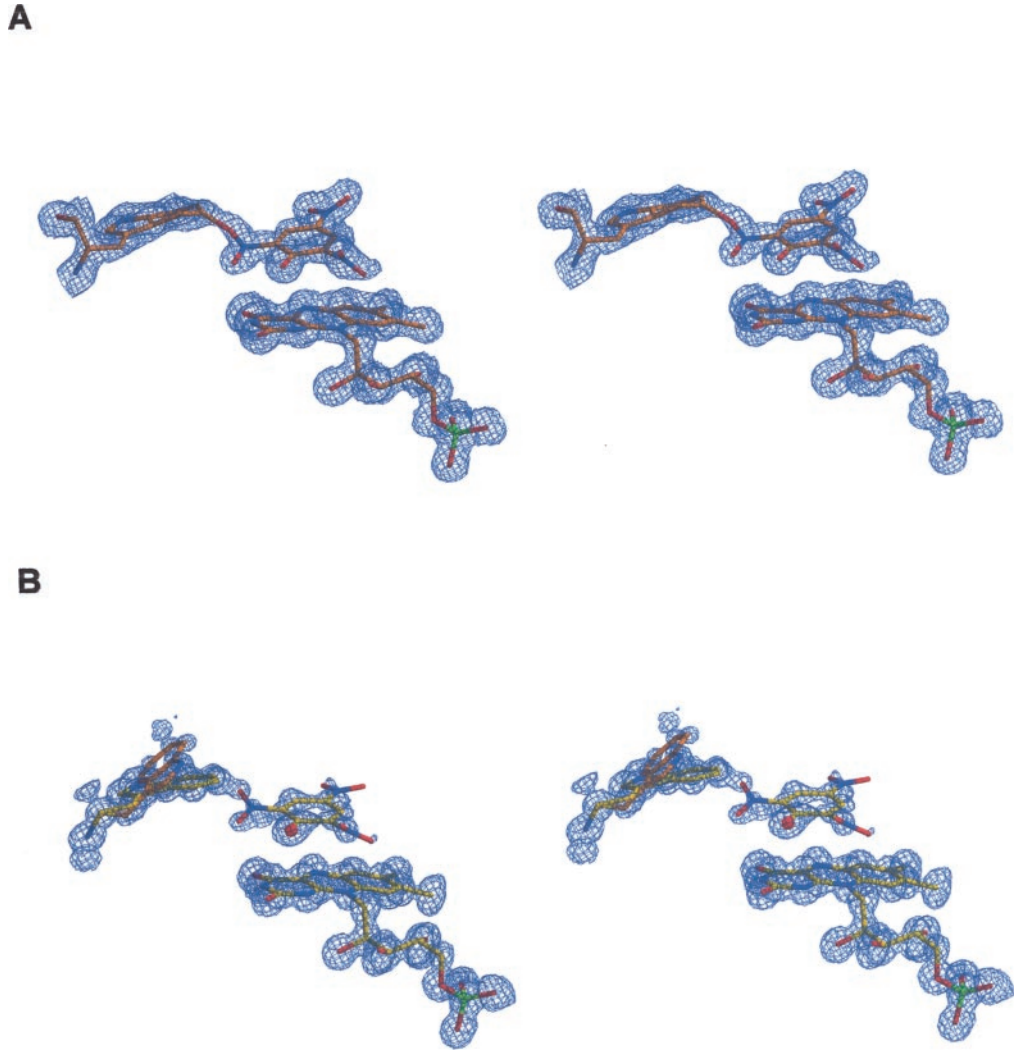

FIG. 2. **Multiple conformational states of Trp-102 in PETN reductase.** *Panel A*, stereo pair of the electron density of Trp-102, picrate, and FMN observed at 1.55 Å, showing the apparent formation of a bond between the nitro group of picrate and the indole of Trp-102. The 6-membered ring appears to have puckered, consistent with the loss of aromatic character. *Panel B*, same view of electron density observed at 0.9 Å, showing that the side chain of Trp-102 adopts two conformations, each with partial occupancy, thus avoiding a steric clash with the partially occupied picrate.

reductase in complex with picric acid were grown in the manner described previously for wild-type PETN reductase (2, 14). The crystals were isomorphous with those previously described, having space group $P2_12_12_1$ and one molecule per asymmetric unit. Data for the wild-type and W102Y mutants were collected at the Daresbury Synchrotron Radiation Source (Daresbury, UK) and data for the W102F enzyme were collected at the European Synchrotron Radiation Facility (Grenoble, France). The data were measured and reduced with the HKL suite (17). Data collection and processing statistics are given in Table I. The mutant structures were refined using CNS (18) and Refmac5 (19), but in the refinement of the wild-type enzyme SHELXL (20) was also used. Xtalview (21) was used throughout for the display of electron density and model fitting. Final refinement statistics are given in Table I. The refined structures and diffraction data for the wild-type, W102F, and W012F have been deposited with the Protein Data Bank with accession codes 1vyr, 1vyp, and 1vys, respectively.

RESULTS

Structure of PETN Reductase Bound to Picric Acid at High Resolution—Our previous structural studies of the complex formed between PETN reductase and picric acid at 1.55 Å

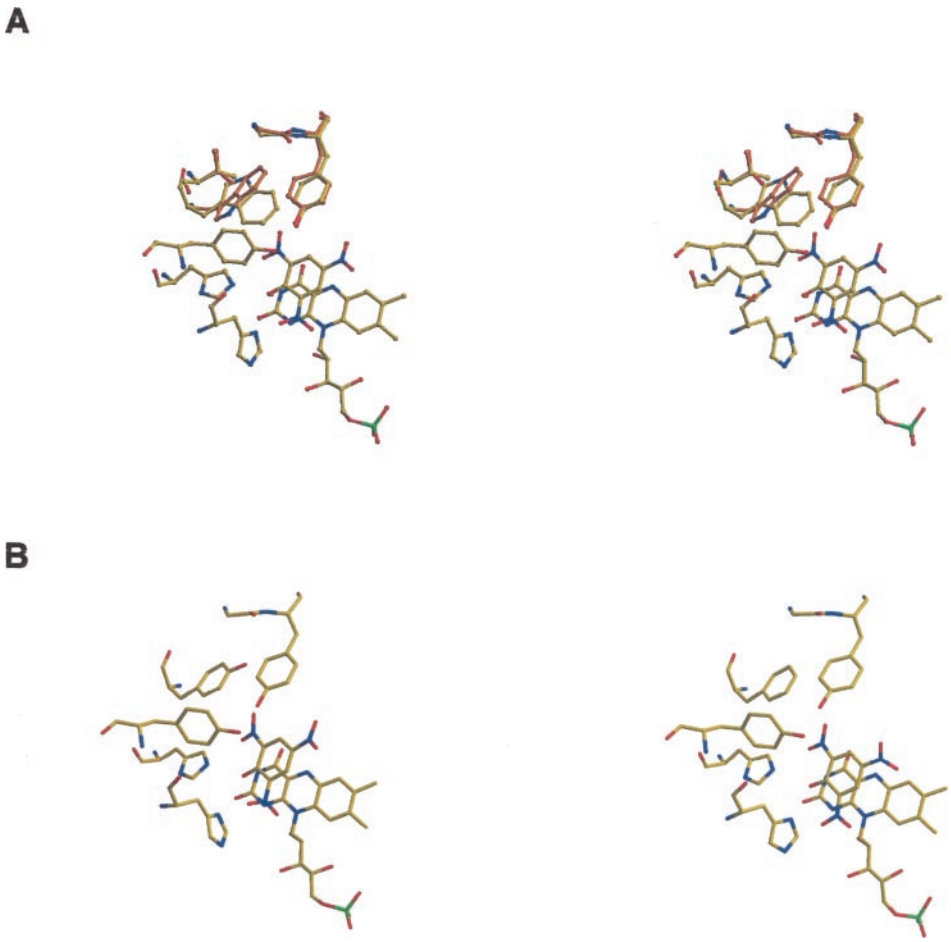

FIG. 3. **Wild-type and mutant PETN reductase active site structures.** *Panel A*, active site structure of PETN reductase determined at high resolution. Stereo pair of the active site of PETN reductase showing the different conformations of residues adjacent to the bound the picrate ligand determined at 0.9 Å resolution. *Panel B*, active site structures of the W102Y (*left panel*) and W102F (*right panel*) mutant enzymes bound to the picrate ligand.

resolution indicated the presence of additional density between the indole side chain of Trp-102 and the C-6 nitro group of picric acid (14). At subatomic resolution it becomes clear that this density does not represent a covalent bond between the nitroaromatic substrate and protein, but indicates that there are at least two conformations of the side chain of Trp-102 (Fig. 2). One of these conformations overlaps with bound picric acid. The occupancy of the picric acid and the non-overlapping conformer of Trp-102 is estimated at 33%. The electron density of the 1.55 Å structure is compared with that of the resolved structure in Fig. 2. Comparison with the structures of PETN reductase in complex with smaller ligands such as 2,4-dinitrophenol (14) suggests that, upon binding picric acid, the side chain of Trp-102 moves to accommodate the bulky nitro group at C-6. The relatively low occupancy of the picric acid leads to an apparent connection between the electron densities even at near-atomic resolution. The electron density of the minor conformation was initially interpreted as evidence for the lack of planarity of the indole side chain of Trp-102, which would be expected upon formation of a link between picric acid and the indole side chain but, as demonstrated herein, extension to high resolution indicates that this is not the case.

The multiple conformations of Trp-102 have a further effect on the side chain of Thr-104, which is seen to adopt two conformations. Tyr-68, which is also involved in formation of the active site is also seen to adopt two conformations about chi-2; these multiple conformations are seen to extend as far as the main chain of Gly-67 (Fig. 3). The side chain of Ser-132, distal to the active site from Tyr-68, is also seen to have two conformations. There are also other regions of the enzyme away from the active site where multiple conformations are found, which is consistent with observations made with other structures reported at subatomic resolution (*e.g.* Ref. 22). In particular, methionine and proline show as mixed conformational populations. There is also evidence for the radiation-induced decarboxylation of some amino acid residue side chains and the carboxyl-terminal group as reported by Ravelli and McSweeny (23); deamination of some side chains is also seen at a lower level.

Crystallographic Structures of the W102Y and W102F Enzyme-Ligand Complexes and Ligand Binding to W102Y and W102F Enzymes—In contrast to the multiple conformations found in the active site of the wild-type enzyme, the W102F and W102Y mutant enzymes, where a potential steric clash upon picrate binding has been removed by engineering, show no evidence for multiple conformations of the residues in the active site. Furthermore, the picric acid appears to fully occupy the active site. The active sites of the mutants are shown in Fig. 3*B*. The mutations at residue 102 have not introduced any other significant alteration. The structures suggest that the nitro group at C-6 of picric acid is accommodated without steric clash, which should favor binding of picric acid (and by inference TNT which is likely to bind in a similar mode, Ref. 14) in the active site of PETN reductase.

The binding of nitroaromatic compounds (picric acid and TNT) to wild-type and mutant forms of PETN reductase was

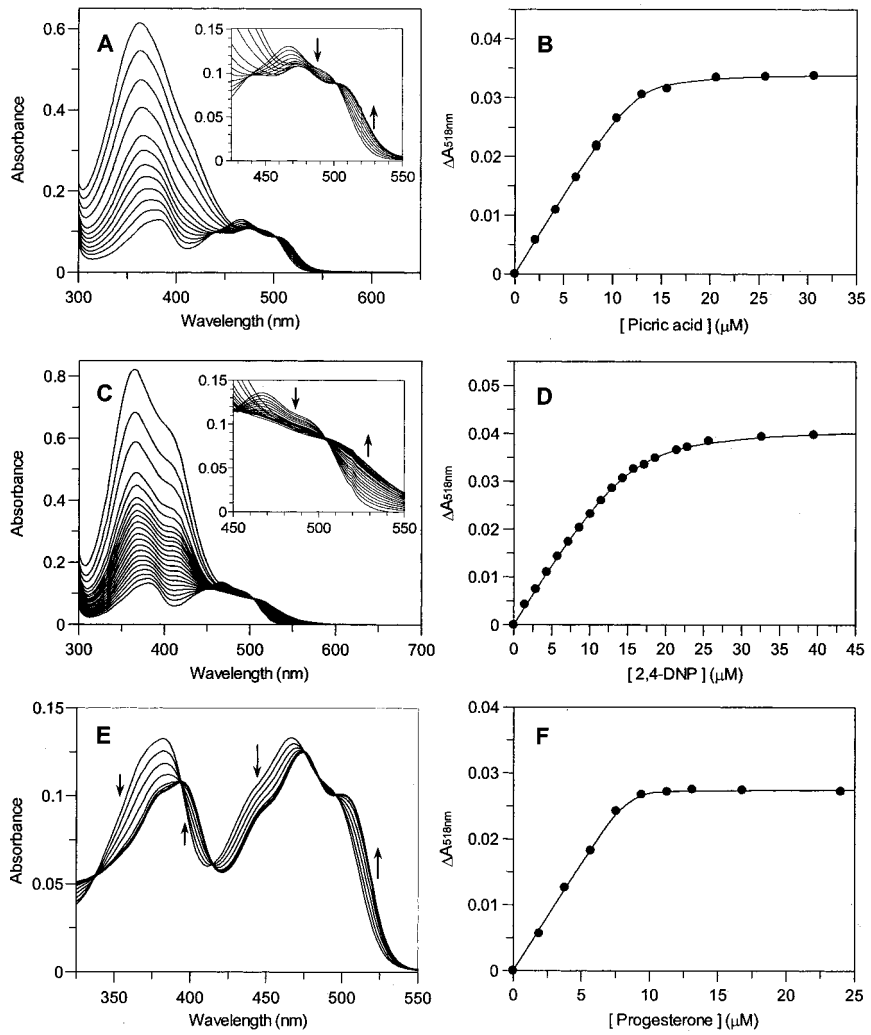

FIG. 4. **Titrations of W102Y PETN reductase with picric acid, 2,4-DNP, and progesterone.** Conditions: 50 mM potassium phosphate buffer, pH 7.0, 25 °C.; enzyme concentration was 10 μM. *Panel A*, spectral changes observed on titrating W102Y PETN reductase with picric acid. *Inset*, detail for the region of 500–525 nm. *Panel B*, plot of absorbance change at 518 nm *versus* picric acid concentration. The *solid line* indicates the fit to Equation 1. *Panels C* and *D*, as for *panels A* and *B*, but for titration of W102Y PETN reductase with 2,4-DNP. *Panels E* and *F*, as for *panels A* and *B*, but for titration of W102Y PETN reductase with progesterone. Similar spectral titrations were obtained with the W102F mutant enzyme. Enzyme-ligand dissociation constants are collected in Table II.

investigated by perturbation of the electronic absorption spectrum of the enzyme-bound FMN. Equilibrium binding measurements with wild-type PETN reductase have been reported (14), and an identical approach was used with the mutant enzymes. Addition of picric acid and 2,4-DNP to the mutant PETN reductase enzymes elicited changes in the electronic absorption spectrum with well defined isosbestic points (Fig. 4) and enzyme-ligand dissociation constants were calculated by fitting data obtained at 518 nm to Equation 1. Enzyme-ligand dissociation constants are collected in Table II. With picric acid, the dissociation constants indicate tighter binding of the ligand to the mutant enzymes compared with wild-type PETN reductase. The wild-type and mutant enzymes have similar affinities for 2,4-DNP. These observations are consistent with the crystallographic data, which indicate a steric interaction between the side chain of Trp-102 and one of the nitro groups of picric acid, but not 2,4-DNP. Titrations were also performed with progesterone, an inhibitor of PETN reductase that also elicits spectral changes on binding in the active site (14). In this case, the dissociation constant for the progesterone-enzyme complex is not affected by mutation, which is consistent with the lack of interaction between Trp-102 and progesterone in the crystal structure of the steroid-enzyme complex (2). As with wild-type PETN reductase (14), the addition of TNT to the W102Y and W102F enzymes did not elicit spectral change, suggesting weak binding of this ligand is attributed to poor interaction of the methyl group of TNT with His-181 and His-184. These latter residues form strong interactions with the hydroxy group of picric acid, which is replaced by a methyl group in TNT.

TABLE II
Calculated dissociation constants for wild-type, W102F, and W102Y PETN reductases

Wild-type PETN reductase and W102F and W102Y mutant enzymes (10 μM) were each titrated with picric acid, progesterone, and 2,4-DNP in 50 mM sodium phosphate buffer, pH 7.0, 25 °C. Data at 518 nm were plotted as a function of ligand concentration and fitted using Equation 1 (see Fig. 4, *panels B*, *D*, and *F* for the W102Y enzyme).

Ligand	Dissociation constant (K_d) for each ligand-PETN reductase complex		
	Wild-type	W102F	W102Y
	μM	μM	μM
Picric acid	5.4 ± 1.1	0.07 ± 0.03	0.24 ± 0.04
Progesterone	0.07 ± 0.03	0.07 ± 0.04	0.03 ± 0.02
2,4-DNP	0.95 ± 0.13	0.21 ± 0.12	1.05 ± 0.09

Kinetic Analysis of the Reductive and Oxidative Half-reactions of W102Y and W102F PETN Reductases—The kinetic mechanism for the reductive half-reaction of wild-type PETN reductase has been described elsewhere (14) and involves the formation of an enzyme-NADPH charge-transfer complex (E-NADPH) followed by enzyme reduction (Scheme 1). The rate of formation and decay of the charge-transfer complex for the mutant enzymes was measured in stopped-flow studies with absorption detection at 560 nm (Fig. 5). Reduction of the flavin was monitored at 464 nm as a single exponential decrease in

$$E_{ox} + NADPH \underset{k_{-1}}{\overset{k_1}{\rightleftharpoons}} E_{ox}NADPH \underset{k_{-2}}{\overset{k_2}{\rightleftharpoons}} E_{red}NADP^+ \underset{k_{-3}}{\overset{k_3}{\rightleftharpoons}} E_{red} + NADP^+$$

SCHEME 1

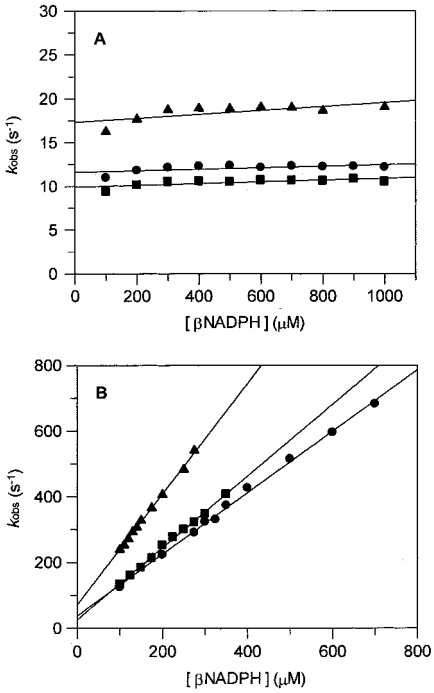

FIG. 5. **Plot of observed rate constants against NADPH concentration for the reaction of wild-type, W102F, and W102Y PETN reductases.** *Panel A*, plot of observed rate constants obtained from analysis of the decrease in absorption at 464 nm against NADPH concentration. *Panel B*, plot of observed rate constants obtained from analysis of the increase in absorption at 560 nm (formation of the charge-transfer intermediate) against NADPH concentration. Kinetic parameters obtained from these plots are collected in Table III. Conditions: 50 mM potassium phosphate buffer, pH 7.0, 5 °C, 20 μM PETN reductase. Symbols: *circles*, wild-type PETN reductase; *squares*, W102Y PETN reductase; *triangles*, W102F PETN reductase.

absorbance and was shown to be kinetically equivalent to the slow-down phase observed in the biphasic transients observed at 560 nm. As with wild-type PETN reductase (14), the rate of flavin reduction for the mutant enzymes was essentially independent of NADPH concentration (range 100–1000 μM coenzyme) at 5 °C (Fig. 5*A*). Global analysis of photodiode array data has indicated that flavin reduction is essentially irreversible in wild-type PETN reductase (*i.e.* $k_{-2} \sim 0$; see Ref. 15 for more detailed discussion), and similar observations were made for the W102Y and W102F enzymes by global fitting of spectral data sets obtained in stopped-flow studies of the reductive half-reaction (data not shown). Consistent with the kinetic model proposed for wild-type enzyme (Scheme 1), charge-transfer complex (E-NADPH) formation in the mutant enzymes is dependent on NADPH concentration and is reversible (Fig. 5*B*). Rate constants for formation and decay of the charge-transfer complex and for flavin reduction are given in Table III. From these data it is clear that mutation of Trp-102 does not substantially affect the rate of flavin reduction by NADPH or the rate of formation and decay of the E-NADPH charge-transfer species, although a modest ~2-fold increase in the hydride transfer rate and the rate of decay of the enzyme-NADPH complex is seen with the W102F PETN reductase.

Kinetic parameters for the oxidative half-reaction of the W102Y and W102F PETN reductases with the nitroester substrate GTN and the nitroaromatic substrate TNT were investigated by mixing dithionite-reduced enzyme titrated with the oxidizing substrate as described previously for wild-type enzyme (14). Rate constants and apparent enzyme substrate dissociation constants are given in Table III. Exchange of Trp-102 for tyrosine and phenylalanine enhances the binding of GTN to reduced enzyme, although in the W102F PETN reductase the limiting rate of flavin oxidation is substantially impaired (~10-fold). The impaired rate of flavin reoxidation is likely not attributed to changes in the midpoint reduction potential of the flavin. Potentiometric studies revealed that the FMN cofactor in the W102F enzyme is, like the wild-type and W102Y enzymes, reduced in a concerted two-electron fashion. The potentials for the two-electron couple are: wild-type PETN reductase (−267 ± 5 mV), W102Y (−236 ± 5 mV), and W102F (−241 ± 5 mV). Although the potential for the FMN cofactor of W102F PETN reductase is ~30 mV more positive than wild-type, it is similar to that of the W102Y enzyme and the flavin re-oxidation kinetics of the W102Y enzyme are similar to wild-type. Thus, it is likely that the impaired rate of FMN re-oxidation in the W102F enzyme is attributed to structural perturbation of the reduced enzyme-GTN complex. Kinetic parameters for flavin oxidation by TNT as measured by the rate of absorption increase at 464 nm (*i.e.* flavin oxidation) on mixing dithionite-reduced enzyme with TNT are only modestly affected by mutation (Table III).

Photodiode array analysis of the oxidation of wild-type PETN reductase by TNT indicates an increase in absorption at ~560

TABLE III
Rate constants for the reductive and oxidative half-reactions of wild-type PETN reductase and the W102Y and W102F mutant enzymes

Stopped-flow reactions were performed by mixing each enzyme (20 μM). Reactants were contained in 50 mM potassium phosphate buffer, pH 7.0. Flavin reduction and oxidation was followed at 464 nm, and the rate of formation of the charge-transfer complex (reductive half-reaction) was followed at 560 nm. Absorption transients were fitted to appropriate rate equations as described. In the reductive half-reaction, observed rate constants (k_{obs}) were analyzed as a function of NADPH concentration to derive values for k_1, k_{-1} and k_2. k_1 is the rate constant for the formation of the charge-transfer complex; k_{-1} is the dissociation rate constant of this complex. k_2 is the rate constant of flavin reduction. K_d is the apparent dissociation constant for NADPH and enzyme calculated as k_{-1}/k_1. In the oxidative half-reaction, k_{lim} is the limiting rate constant for flavin oxidation and K_d is the apparent dissociation constant for the complex formed between reduced enzyme and the oxidizing substrate.

Reductive half-reaction	k_1	k_{-1}	k_2	K_d
	$\mu M^{-1}\ s^{-1}$	s^{-1}	s^{-1}	μM
Enzyme				
Wild-type[a]	0.95 ± 0.02	32.7 ± 7.4	11. 0.2	33.3 ± 8.5
W102F	1.68 ± 0.02	70.9 ± 4.4	17.3 ± 0.5	42.2 ± 3.1
W102Y	1.09 ± 0.01	25.7 ± 4.5	9.9 ± 0.2	23.5 ± 4.3

Oxidative half-reaction	GTN		TNT	
	k_{lim}	K_d	k_{lim}	K_d
	s^{-1}	mM	s^{-1}	mM
Enzyme				
Wild-type[a]	518 ± 51	1.5 ± 0.3	4.5 ± 0.1	0.09 ± 0.01
W102F	52 ± 3.1	0.28 ± 0.04	6.0 ± 0.4	0.16 ± 0.03
W102Y	322 ± 18.7	0.22 ± 0.04	13 ± 0.5	0.23 ± 0.02

[a] Values for the wild-type enzyme are taken from Ref. 14.

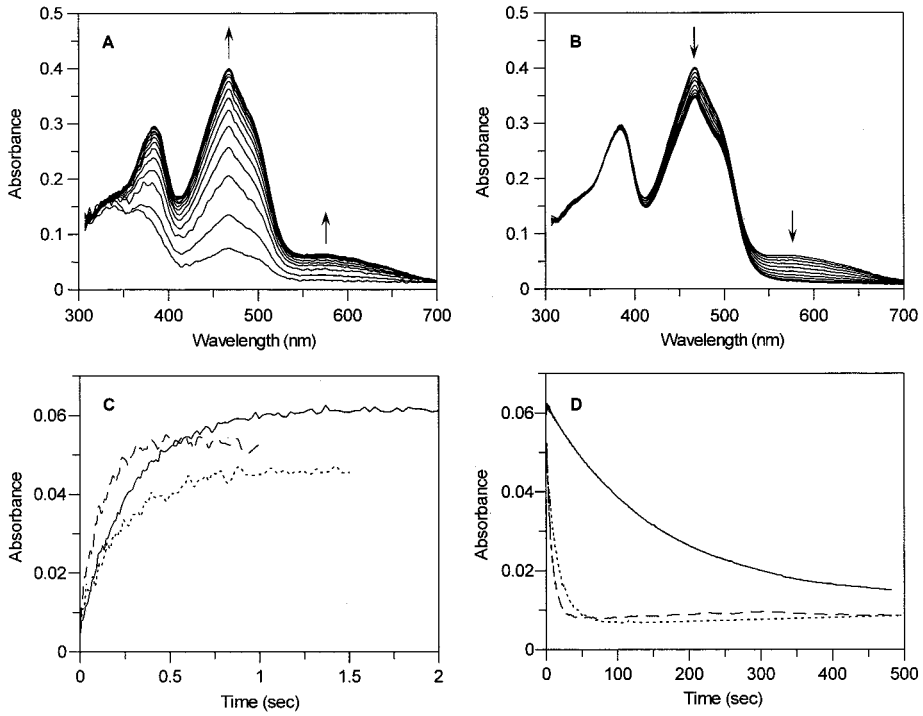

FIG. 6. **Photodiode array and single wavelength stopped-flow analysis analysis of the oxidative half-reaction of PETN reductase with TNT as substrate.** *Panel A*, spectra obtained on mixing dithionite-reduced W102Y PETN reductase with TNT over 5 s from the mixing event. The increase in absorption at ~560 nm indicates formation of the hydride-Meisenheimer complex, and the increase in absorption at 460 nm indicates oxidation of the FMN. Data were collected using a log time scale, and for clarity only every 5th acquired spectrum is shown. *Panel B*, as for *panel A*, except spectra shown are for data acquisition in the 1–100 s time domain after mixing (log time base; every 25th spectrum illustrated). The decrease in absorption at 560 nm indicates decay of the hydride-Meisenheimer complex. *Panel C*, single wavelength kinetic transients obtained at 560 nm indicating formation of the hydride-Meisenheimer complex with wild-type, W102Y, and W102F PETN reductases. *Solid line*, wild-type enzyme (k_{obs} 3.6 s^{-1}); *dashed line*, W102Y enzyme (k_{obs} 4.0 s^{-1}); *dotted line*, W102F enzyme (k_{obs} 8.5 s^{-1}). *Panel D*, single wavelength kinetic transients for decay of the hydride-Meisenheimer complex in wild-type, W102Y, and W102F PETN reductases. *Solid line*, wild-type enzyme (k_{obs} 0.006 s^{-1}); *dashed line*, W102Y enzyme (k_{obs} 0.14 s^{-1}); *dotted line*, W102F enzyme (k_{obs} 0.06 s^{-1}). Conditions: 50 mM potassium phosphate buffer, pH 7.0, 25 °C, 35 μM PETN reductase, 350 μM TNT.

nm concomitant with flavin re-oxidation, which indicates the formation of the hydride-Meisenheimer complex (14). Over extended timescales, the absorption at ~560 nm decreases indicating decay of the hydride-Meisenheimer complex. Analysis with the W102Y and W102F PETN reductases likewise indicated formation and decay of the hydride-Meisenheimer complex (Fig. 6, *A* and *B*), and the maximum absorption at 560 nm for both the W102Y and W102F enzymes (Fig. 6*A*) is similar to that observed for the wild-type enzyme (14). Single wavelength stopped-flow analysis at 560 nm indicated that formation of the Meisenheimer hydride complex occurs with similar kinetics in wild-type, W102Y, and W102F PETN reductases (Fig. 6*C*), which is consistent with data obtained at 464 nm that monitors flavin oxidation (Table III) and the fact that flavin oxidation and formation of the Meisenheimer-hydride complex is concerted. However, decay of the Meisenheimer-hydride complex was much more rapid (> 10-fold increase in the observed rate constant) with the W102Y and W102F PETN reductases compared with the wild-type enzyme (Fig. 6*D*), indicating that decay of the Meisenheimer-hydride complex is an enzyme-catalyzed process.

Multiple Turnover Studies with TNT—The spectral characteristics of the reaction products that accumulate following multiple turnover of wild-type PETN reductase, the W102Y and W102F mutant enzymes are shown in Fig. 7. In each case, reactions were allowed to proceed until a stable final spectrum was produced. The spectral properties of the reaction products for wild-type PETN reductase are clearly very different from those of the two mutant enzymes, suggesting either (i) the accumulation of different reaction products or (ii) a different distribution of multiple reaction products. Multiple pathways are available to PETN reductase for reduction of TNT (Ref. 13; see below for more detailed discussion), which is consistent with either of the above possibilities. In all cases, it is clear that the Meisenheimer-hydride complex is not accumulated to any large extent, consistent with its breakdown to further products as observed in stopped-flow studies.

Further evidence for the different chemical nature of the reaction products was obtained by NMR spectroscopy. Under anaerobic conditions, one-dimensional NMR spectra were recorded continuously over 3 h, with each spectrum taking 3 min to acquire; the final stable NMR spectrum indicates different reaction products for wild-type and W102Y PETN reductases (Fig. 8). Two-dimensional COSY spectra (not shown) for the wild-type and W102Y reactions allowed the identification of peaks that arise from the same functional groups (*e.g.* the number of CH_2 groups); these are denoted by numbers 1–4 in Fig. 8. The one- and two-dimensional NMR spectra recorded at the end of the 3-h reaction time indicated a more complex mixture of compounds for the wild-type enzyme compared with the W102Y PETN reductase. Spectral peaks that arise during the full course of the reaction were then analyzed for their pattern of development as a function of time. Analyses revealed that different peaks form and decay at differing times and that the decay of some peaks leads to the concomitant formation of others. Overall, the results of these NMR studies reveal that a number of intermediates are produced during TNT turnover and that these differ either in their nature or in their proportionate accumulation, between wild-type and W102Y PETN reductase. At this stage, it is not

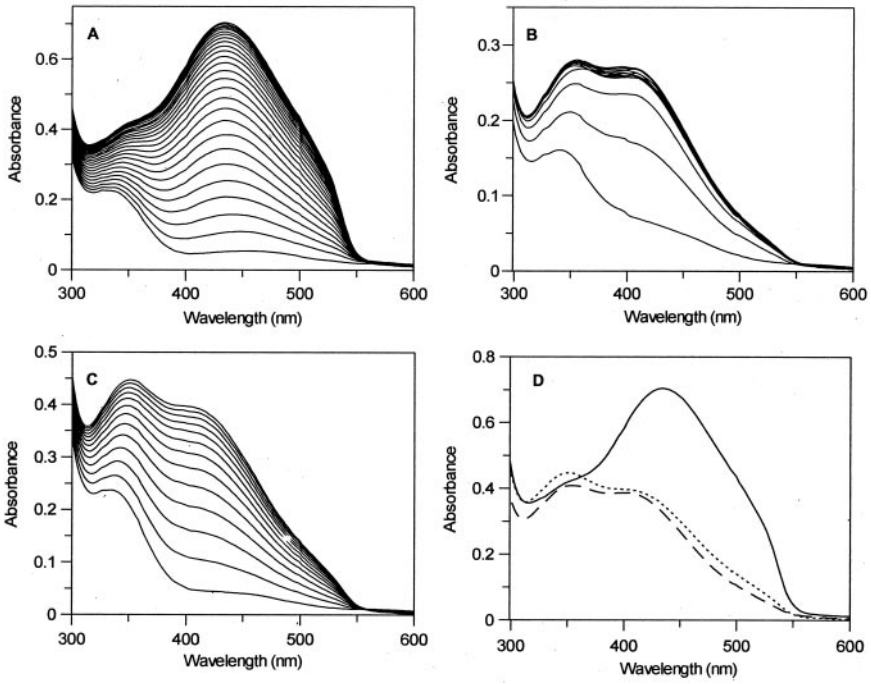

FIG. 7. **Spectra obtained during multiple turnover of PETN reductase with TNT.** *Panel A*, spectra obtained with wild-type PETN reductase. *Panel B*, spectra obtained with W102Y PETN reductase. *Panel C*, spectra obtained with W102F PETN reductase. *Panel D*, final spectra obtained in each of the reactions shown in *panels A–C*. Wild-type, *solid line*; W102Y, *dashed line*; W102F, *dotted line*. Conditions: 50 mM potassium phosphate buffer, pH 7, 25 °C; 0.2 μM PETN reductase; 88 μM TNT; 10 mM glucose 6-phosphate; 100 μM NADPH; 1 unit of glucose-6-phosphate dehydrogenase. Individual spectra were acquired every 2 min (wild-type and W102F) and 4 min (W102Y) following initiation of the reaction.

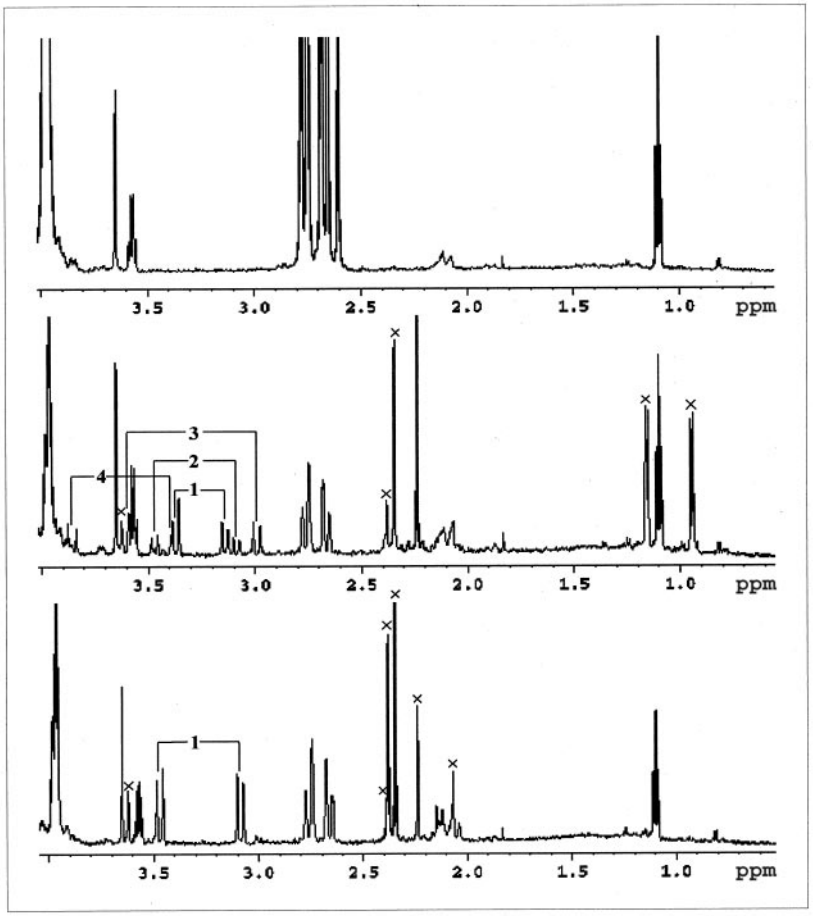

FIG. 8. **Analysis of the products of multiple turnover of wild-type and W102Y PETN reductases by NMR spectroscopy.** NMR analysis was used to follow the reaction between 0.2 μM enzyme, 1.5 mM NADPH, and 1 mM TNT (in 99.9% D_2O acetone), in 50 mM D_2O phosphate buffer, pH7.0. The spectra displayed correspond to the final spectrum recorded after the reaction was left for 3 h. The *numbers* correspond to the formation of peaks, which arise from the same CH_2 groups, identified by the two-dimensional COSY spectrum for each reaction. *X* highlights the peaks that form during the course of the reaction that exclude signals from NADPH, $NADP^+$ (which has a signal at ~2.15 ppm), and TNT. The NMR spectrum for NADPH plus TNT is also displayed for comparative purposes. *Upper spectrum*, NADPH (1.5 mM) and TNT (1 mM) alone; *middle spectrum*, for wild-type PETN reductase; *lower spectrum*, for W102Y PETN reductase.

possible to determine the identity of the compounds produced during the course of the reaction as the complexity of the spectra (because of the presence of many different compounds) prevents the assignment of spectral peaks. This aspect is the focus of future work.

DISCUSSION

The structure of the wild-type enzyme in complex with picric acid shows that the apparent link seen between the nitro group of the substrate and Trp-102 at 1.55 Å is due to the limited resolution of the electron density. At 0.9 Å the multiple confor-

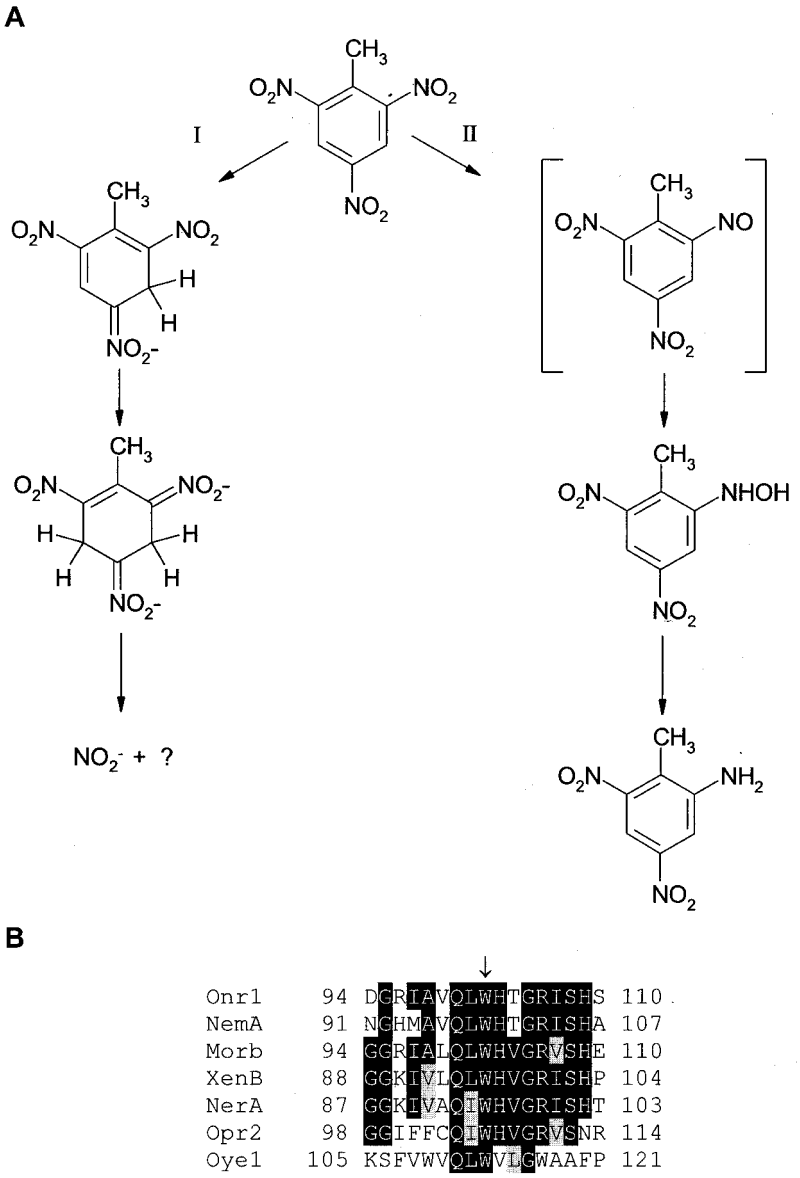

FIG. 9. **Parallel pathways for TNT degradation by PETN reductase.** *Panel A*, transformation of TNT by PETN reductase. Each step requires the oxidation of one equivalent of NADPH. For further details see Ref. 13. *Panel B*, multiple sequence alignment of proteins related to PETN reductase centered on the region surrounding conserved tryptophan 102 (denoted by ↓) from PETN reductase. Sequences are as follows: *E. cloacae* PETN reductase, Onr1; *E. coli N*-ethylmaleimide reductase, NemA; *P. putida* morphinone reductase, MorB; *Agrobacterium tumefaciens* GTN reductase, NerA; *Pseudomonas fluorescens* 1-C xenobiotic reductase B, XenB; *Arabidopsis thaliana* 12-oxophytodienoate reductase, Opr2; *S. cerevisiae* old yellow enzyme, Oye1.

mations of the side chain are resolved and the apparent link is seen as the super-position of two different structures. The lack of changes in the structures of the W102Y and W102F structures validate the assumptions implicit in the ligand binding (Fig. 4 and Table II) and reductive half-reaction kinetic studies (Fig. 5) of the mutants, *i.e.* there are no other changes in the structure apart from those at the site of the mutation. These structural results show clearly that the active site of PETN reductase is sufficiently malleable to accommodate more bulky substrates than would be expected to fit into a rigid active site. Specifically, the conformational mobility of Trp-102 is key to relieving any steric clash between the C-6 nitro group of picric acid (and by inference TNT) and the side chain of Trp-102; the well defined electron density for Tyr-102 and Phe-102 in the crystal structures of the W102Y and W102F enzymes is consistent with the ability of these enzymes to accommodate the C-6 nitro group of picric acid in the absence of a steric clash with the engineered side chains.

In previous work we have demonstrated that the degradation of TNT by wild-type PETN reductase in multiple turnover assays follows two competing pathways involving (i) formation and subsequent decay of the Meisenheimer-hydride and Meisenheimer-dihydride complexes of TNT and (ii) reduction of the nitro groups of TNT in a conventional nitroreductase reaction (Fig. 9*A*, *pathways I* and *II*, respectively). The final products of both these pathways are as yet unknown, but nitroso- and hydroxylamino metabolites (formed in the nitroreductase pathway) have the potential to polymerize to form azoxy dimers (24, 25). The possibility of abiotic condensation of the Meisenheimer-dihydride complex and hydroxylamino-dinitrotoluenes has been considered in biotransformations with xenobiotic reductase B, an enzyme that is a close orthologue of PETN reductase isolated from *Pseudomonas fluorescens* 1-C (12). With PETN reductase, nitrite is known to be a product of the pathway that involves formation and decay of the Meisenheimer-hydride complexes, but the final products have not been identified. The chemically synthesized Meisenheimer-hydride complex of TNT is converted to the Meisenheimer-dihydride complex by PETN reductase and then to unknown products, without formation of hydroxylamino-dinitrotoluenes or amino-dinitrotoluenes (13). In this earlier study we demonstrated that His-184 is critical for orientating TNT in the active site for hydride transfer to the aromatic ring. Our stopped-flow studies with the W102Y and W102F PETN reductases indicate that rate constants for decay of the Meisenheimer-hydride complexes are substantially faster than with wild-type PETN re-

ductase (Fig. 6*D*). This observation demonstrates unequivocally that decay of the Meisenheimer-hydride complex is enzyme catalyzed, a finding that is consistent with our previous multiple turnover analysis with different concentrations of wild-type PETN reductase (13).

Residue Trp-102 of PETN reductase is conserved throughout the sequence-related old yellow enzyme family of enzymes (Fig. 9*B*). The activity of a number of these enzymes has been investigated with TNT as substrate (13). All of the enzymes studied (*E. cloacae* PB2 PETN reductase, *E. cloacae* type-strain (ATCC13047) PETN reductase, *Escherichia coli N*-ethyl maleimide reductase, *Pseudomonas putida* M10 morphinone reductase and *Saccharomyces carlsbergensis* old yellow enzyme) showed some activity with TNT in multiple turnover assays. However, only the *E. cloacae* and *E. coli* enzymes gave rise to an orange-colored product, suggesting that only these enzymes can transform TNT to form dihydride products (Fig. 9*A*, *pathway I*). HPLC analysis of reaction products confirmed that each enzyme possesses nitroreductase activity (pathway II), but that the direct hydride transfer pathway is restricted to the *E. cloacae* and *E. coli* enzymes. Interestingly, old yellow enzyme was found not to transform TNT to orange-colored products, but it was able to convert chemically synthesized Meisenheimer-hydride complex to the Meisenheimer-dihydride product and further to the uncharacterized reaction products, indicating the partial operation of pathway I in this enzyme (13). Our data presented in this report reveal that Trp-102 is a key determinant in binding nitroaromatic substrates and that it influences the chemical nature of the products accumulated under multiple turnover conditions. Mutagenesis of Trp-102 (to Tyr-102 and Phe-102) does not affect the ability of PETN reductase to accumulate the Meisenheimer-hydride complex of pathway I (Fig. 9) in single turnover stopped-flow studies, but strikingly this intermediate is kinetically much less stable than in reactions performed with wild-type enzyme. This kinetic imbalance between the wild-type and mutant enzymes is sufficient to generate a different and less complex distribution of reaction products for the mutant enzymes, which perhaps reflects more favored partitioning along pathway I for these enzymes. Given the striking affect of the W102Y and W102F mutations and the overall structural similarity of the old yellow enzyme family members, our results suggest that small modifications in active site structure (centered around the conserved tryptophan residue) could modulate the balance between the two pathways for nitroaromatic transformation. This potentially opens up the exciting prospect of engineering old yellow enzyme and other family members that operate (almost) exclusively via pathways II, to transform nitroaromatic substrates using the hydride transfer pathway (pathway I).

Concluding Remarks—The atomic structure of the wild-type PETN-reductase-picric acid complex indicates multiple conformational states for Trp-102 as a result of a steric clash between the side chain of this residue and the C6 nitro group of picric acid. This steric constraint is relieved in the W102Y and W102F enzymes and is reflected in tighter binding of picric acid to the mutant enzymes. Mutation of Trp-102 has very minor effects on the overall active site structure of the enzyme, but the small structural changes induced are sufficient to accelerate the decay of the Meisenheimer-hydride complex formed in pathway I. That decay of the Meisenheimer-hydride complex is accelerated on mutation establishes unequivocally that this reaction is enzyme catalyzed. The study emphasizes that small structural changes induced by mutation can have a profound effect on active site chemistry and kinetics and further opens up the possibility of engineering new activities in those old yellow enzyme family members that do not transform TNT via pathway I.

REFERENCES

1. Binks, P. R., French, C. E., Nicklin, S., and Bruce, N. C. (1996) *Appl. Environ. Microbiol.* **62,** 1214–1219
2. Barna, T. M., Khan, H., Bruce, N. C., Barsukov, I., Scrutton, N. S., and Moody, P. C. (2001) *J. Mol. Biol.* **310,** 433–447
3. Fox, K. M., and Karplus, P. A. (1994) *Structure* **2,** 1089–1105
4. Barna, T., Messiha, H. L., Petosa, C., Bruce, N. C., Scrutton, N. S., and Moody, P. C. (2002) *J. Biol. Chem.* **277,** 30976–30983
5. French, C. E., and Bruce, N. C. (1995) *Biochem. J.* **312,** 671–678
6. French, C. E., Nicklin, S., and Bruce, N. C. (1996) *J. Bacteriol.* **178,** 6623–6627
7. Blehert, D. S., Fox, B. G., and Chambliss, G. H. (1999) *J. Bacteriol.* **181,** 6254–6263
8. Snape, J. R., Walkley, N. A., Morby, A. P., Nicklin, S., and White, G. F. (1997) *J. Bacteriol.* **179,** 7796–7802
9. French, C. E., Nicklin, S., and Bruce, N. C. (1998) *Appl. Environ. Microbiol.* **64,** 2864–2868
10. Williams, R. E., Rathbone, D., Bruce, N. C., Scrutton, N. S., Moody, P. C. E., and Nicklin, S. (1999) in *Flavins and Flavoproteins* (Ghisla, S., Kroneck, P., Macheroux, P., and Sund, H., eds) pp. 663–666, Rudolf Weber, Berlin
11. Williams, R., Rathbone, D., Moody, P., Scrutton, N., and Bruce, N. (2001) *Biochem. Soc. Symp.* **8,** 143–153
12. Pak, J. W., Knoke, K. L., Noguera, D. R., Fox, B. G., and Chambliss, G. H. (2000) *Appl. Environ. Microbiol.* **66,** 4742–4750
13. Williams, R. E., Rathbone, D. A., Scrutton, N. S., and Bruce, N. C. (2004). *Appl. Environ. Microbiol.*, in press
14. Khan, H., Harris, R. J., Barna, T., Craig, D. H., Bruce, N. C., Munro, A. W., Moody, P. C., and Scrutton, N. S. (2002) *J. Biol. Chem.* **277,** 21906–21912
15. Basran, J., Harris, R. J., Sutcliffe, M. J., and Scrutton, N. S. (2003) *J. Biol. Chem.* **278,** 43973–43982
16. Sambrook, J., Fritsch, E., and Maniatis, T. (1989) *Molecular Cloning: A Laboratory Manual*, 2nd Ed., Cold Spring Harbor Laboratory Press, Cold Spring Harbor, NY
17. Otwinowski, Z., and Minor W. (1997) *Methods Enzymol.* **276,** 307–326
18. Brunger, A., Adams, P., Clore, G., DeLano, W., Gros, P., Grosse-Kunstleve, R., Jiang, J.-S., Kuszewski, J., Nilges, M., Pannu, N., Read, R., Rice, L., Simonson, T., and Warren, G. (1998). *Acta Crystallogr. Sect. D* **54,** 905–929
19. Murshudov, G., Vagin, A., and Dodson, E. (1997) *Acta Crystallogr. Sect. D* **53,** 240–255
20. Sheldrik, G. M., and Schnieder, T. R. (1997) in *Macromolecular Crystallography, Part B* (Carter, C. W. J., and Sweet, R. M., eds) Vol. 277, pp. 319–343, Academic Press, London
21. McRee, D. (1992) *J. Mol. Graphics* **10,** 44–46
22. Lario, P. I., Sampson, N., and Vrielink, A. (2003) *J. Mol. Biol.* **326,** 1635–1650
23. Ravelli, R. B., and McSweeney, S. M. (2000) *Structure Fold Des.* **8,** 315–328
24. Wang, C., Lyon, D., Hughes, J., and Bennett, G. (2003) *Environ. Sci. Technol.* **37,** 3595–3600
25. Wang, C., Zheng, D., and Hughes, J. (2000) *Biotechnol. Lett.* **22,** 15–19